JOURNAL OF SPACECRAFT AND ROCKETS
Vol. 40, No. 2, March–April 2003

Laboratory Tests on 110-Volt Solar Arrays in Simulated Geosynchronous Orbit Environment

Mengu Cho,* Raju Ramasamy,† Toshiaki Matsumoto,‡ and Kazuhiro Toyoda§
Kyushu Institute of Technology, Kitakyushu 804-8550, Japan
Yukishige Nozaki¶
NEC Toshiba Space Systems, Ltd., Yokohama 224-8555 Japan
and
Masato Takahashi**
National Space Development Agency, Ibaraki 305-8505, Japan

Engineering Test Satellite VIII will be the first Japanese geosynchronous orbit satellite to have 110-V satellite bus voltage, and its solar arrays will generate the electricity at 110 V once it is launched in 2004. Laboratory tests on charging and arcing of the Engineering Test Satellite VIII solar arrays are carried out in a simulated geosynchronous orbit environment irradiating a solar array test coupon with an electron beam in a vacuum chamber. The concept of inverted potential gradient between the coverglass and the interconnector is verified experimentally. Arcs are observed once the potential difference exceeds approximately 400 V. It is confirmed that the sustained arc does not occur between the adjacent array strings as long as silicon rubber grouts the gap between the strings. Another type of sustained arc is observed between the array strings and the aluminum honeycomb substrate through defect on the Kapton® sheet. Based on the test results, modification of the array design is possible.

Nomenclature

C	=	capacitance, F
I_B	=	current to string B, A
I_G	=	current to string G, A
$I_{\max}$	=	maximum current provided by floating power supply, A
I_p	=	negative peak value of langmuir probe signal, A
I_R	=	current to string R, A
R	=	resistance, Ω
V_a	=	bias voltage by floating power supply, V
V_b	=	array bias voltage with respect to the chamber ground, V
ΔV	=	differential voltage between coverglass and interconnector, V
ϕ_a	=	array potential, V
ϕ_{cg}	=	coverglass potential, V
ϕ_{ic}	=	interconnector potential, V

Introduction

SINCE the past decade, the power level of geosynchronous Earth orbit (GEO) satellites has increased dramatically to nearly 10 kW to respond to the demand for carrying more transponders with one satellite. To manage the large amount of power efficiently, the satellite bus voltage has increased to 100 V. Nowadays many U.S. commercial satellites employ solar arrays that generate electricity at 100 V. The National Space Development Agency (NASDA) of Japan plans to launch Engineering Test Satellite VIII (ETS-VIII) in 2004. Figure 1 shows an overview of ETS-VIII in orbit. ETS-VIII is a 3-ton class GEO satellite, and the lifetime is 10 years. In ETS-VIII, new technologies such as high-voltage bus technology (110 V) and large-scale deployable reflector (LDR) made of gold mesh are introduced to establish and verify the technology for future large-scale spacecraft systems. The development of ETS-VIII solar arrays demands careful consideration of the issue of differential charging caused by geomagnetic substorm. Arcing on the solar arrays of ETS-VIII must be studied at the design stage of arrays both theoretically and experimentally.

Arcing on a high-voltage solar array has been studied extensively in the low-Earth-orbit (LEO) environment (Refs. 1–3 and references therein). In LEO, the negative end of a solar array usually has a negative potential, comparable to the array output voltage, with respect to the surrounding plasma. Once the array becomes negative to the plasma, its coverglass is charged by positive ions. The field intensification at the so-called triple junction, where vacuum, conductor (interconnector), and insulator (coverglass) meet, leads to arcing. In GEO, the issue of arcing on a high-voltage solar array has been neglected because the plasma density is lower than LEO by five or six orders of magnitude. In GEO, when a satellite receives sunlight, its charging is dominated by photoelectrons. As long as the satellite surface is well illuminated under the quiet condition, the photoelectrons keep the satellite potential within a few electron volts from the plasma potential. The insulator surface, such as coverglass, has the similar potential. Because the negative end of the solar array is connected to the satellite body that works as the circuit ground, solar array interconnectors have positive potentials with respect to the surrounding plasma.

When a part of the insulator surface is shadowed, its insulator surface can have highly negative potential of approximately 10 kV (Ref. 4), and a large potential difference between the satellite body and the insulator surface can lead to electrostatic discharge. This phenomenon is known as differential charging, and mitigation techniques were developed and implemented in the 1980s (Ref. 5). For the case of differential charging, the insulator surface is more negative than the satellite potential. For the case of the solar array arcing, however, the coverglass potential is less negative than the nearby conductor (interconnector) potential. This potential gradient does not occur under the normal condition. Therefore, this potential gradient is sometimes called an inverted potential gradient.

Even though it is rare, the inverted potential gradient can occur if certain conditions are met. When a satellite encounters a

Presented as Paper 2002-0630 at the 40th Aerospace Sciences Meeting, Reno, NV, 14–17 January 2002; received 19 March 2002; revision received 23 October 2002; accepted for publication 3 November 2002.

*Associate Professor, Department of Electrical Engineering, Tobata-ku; cho@ele.kyutech.ac.jp. Senior Member AIAA.
†Postdoctoral Fellow, Satellite Venture Business Laboratory; currently Postdoctoral Fellow, Department of Electronics, Tokai University, Hiratsuka 259-192, Japan.
‡Graduate Student, Department of Electrical Engineering, Tobata-ku.
§Postdoctoral Fellow, Satellite Venture Business Laboratory, Tobata-ku; toyoda@ele.kyutech.ac.jp.
¶Assistant Manager, Space Systems Department, Business Operation Division, Tsuzuki; nozaki.yukishige@ntspace.jp.
**Associate Senior Engineer, Tsukuba; Takahashi.Masato@nasda.go.jp.

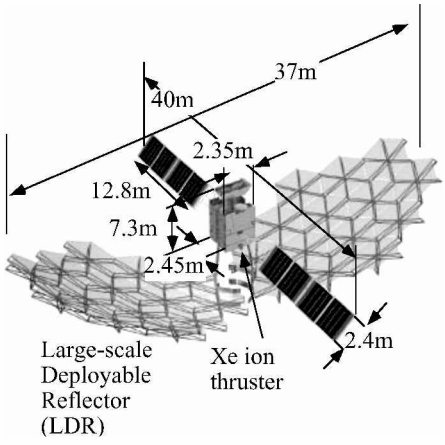

Fig. 1 ETS-VIII satellite in orbit.

geomagnetic substorm, the current due to high-energy electrons increases and sometimes exceeds the current due to photoelectrons.[6] Then the potentials of the satellite body and the insulator surface can become negative. Because of the difference of the secondary electron emission coefficients, the insulator potential may drop more slowly than the satellite body. During that process, the inverted potential gradient may occur at some parts of solar array surface. As the potential difference builds up between the coverglass and the interconnector, an arc may occur. Because a substorm is a natural phenomenon, arcs due to an inverted potential gradient on a solar array probably have occurred through the past decades. The arcs just have been unnoticed or mixed with other electrostatic discharges. Even if an arc occurs, as long as it ends as a single pulse with a small amount of the total energy release, it causes little harm. In this paper, we call this single pulse of arc the trigger arc. The trigger arc on a GEO satellite has attracted little attention while the power generated by each array string is low. However, the risk of one trigger arc growing to a catastrophic arc receiving the energy from the array itself has increased recently as the power level of solar array has increased.

TEMPO-2 satellite experienced the permanent loss of a significant fraction (20%) of solar array output power when a severe substorm hits the satellite in 1997. Katz et al.[6] attributed the failure to an arc on solar array under the inverted potential gradient condition. First, an arc occurred between adjacent array strings with different potential and short circuited the two strings. Then, the array output power of the two strings fed the energy to the arc plasma. The arc current kept flowing, and the underlying Kapton® insulation layer was thermally broken, leading to the short circuit between the array strings and the substrate. In the present paper, we call this type of sustained arc an interstring sustained arc.

Another anomaly probably related with an arc under the inverted potential gradient condition is a sustained arc between the interconnectors and the panel structure, possibly through a insulation defect in the Kapton substrate on which the solar cells are mounted. MARCES-A and ECS-1 experienced partial loss of power, which was attributed to the short circuit between the array and the panel structure through a damaged Kapton sheet.[7] There are several ways for Kapton to be damaged, such as accidental scars caused by workmanship during cell repairing process on the ground or the impact by meteoroids and debris in orbit. Once an arc occurred at the interconnector of the array near the damaged Kapton, a current path may have been formed between the interconnector and the substrate through the damaged portion of the Kapton and led to a short circuit between the interconnector and the substrate and the resultant loss of the power system.[7] We call this type of sustained arc a string–substrate sustained arc in this paper.

Intensive tests were carried out to reproduce the string–substrate sustained arc in laboratory tests. Bogus et al.[7] applied a voltage between 40 and 80 V on 25 μm of a punctured Kapton and carbon fiber sheet and observed the sustained arc. In Ref. 7, the voltage across the Kapton sheet was applied externally, probably by a pair of electrodes. Levy et al.[8] tried to cause the sustained arc by constantly irradiating a solar array coupon with an electron beam. They used a test coupon with no intentional damage inflicted. Trigger arcs were observed, but with the potential difference of as high as 60 V between the string and substrate, the series of trigger arcs did not provoke the string–substrate sustained arc. In the present study, we use a test coupon on which damages are made intentionally and a coupon without any damage. Also the string–substrate voltage is 110 V, considering the maximum potential difference for ETS-VIII employing a 110-V bus voltage compared to the European satellites employing 50-V bus voltage.

The analysis of the surface potentials of the insulating coverglass and the spacecraft body at different positions in GEO orbit such as dawn, noon, midnight (at eclipse), and at the exit of eclipse has been carried out using NASCAP/GEO.[9] The results indicate that at the local morning (0600 hr) the potential difference between the coverglass and the conductive body is as high as 1.2 kV. At noon, the absolute potential of the spacecraft body becomes very close to the space plasma potential, and the charging on the coverglass is very low because the photoemission current from LDR is very large. At midnight, a maximum potential difference of about 2.9 kV is possible between the surface of the coverglass and the conductive body of the satellite. At the exit of the eclipse, the potential of the satellite body is very close to 0 V. The analysis by NASCAP/GEO strongly depends on the secondary electron coefficient of the coverglass. Reducing the maximum secondary electron yield by half results in the potential difference of 500 V, instead of 1.2 kV, at the local morning. To avoid the uncertainty associated with the material property data, the secondary electron yield of ZrO_2, the coating material of coverglass, was measured by Kawakita et al.[10]

In this report, we present the experimental studies on the test of solar arrays of the ETS-VIII in a simulated GEO environment with electron beam exposure on the array surface. We focus our tests on the inverted potential gradient condition. First, we verify whether the inverted potential gradient is possible by irradiating solar array by an electron beam, where the array is completely floating from the chamber ground. Then, we carry out the experiment by creating the inverted potential gradient by biasing the array to a high negative potential (of the order of magnitude of kilovolts) using a high-voltage power supply and making the potential of the coverglass of the array less negative. We examine the trigger arc inception on the solar array at the inverted potential gradient and find the threshold voltage for the trigger arc initiation.

We also examine whether the interstring sustained arc occurs between adjacent cells of the array at the potential difference of 55 V with a current capability of 2.64 A, which is the maximum condition of ETS-VIII. In the ground-based experiments, we cannot test the full string of solar array of the satellite. Therefore, we insert the additional capacitance into the test system to increase the energy release and to examine whether that condition leads to the sustained arc. To study the string–substrate sustained arc, we intentionally damage the Kapton insulating film on which solar cells are mounted and examine whether the string–substrate sustained arc occurs or not. We also test a healthy coupon and examine whether the repeated trigger arcs lead to the damage to the Kapton sheet and the string–substrate sustained arc. Finally, we propose the modification of the array design.

We first describe the laboratory experiments, which simulate the interaction of solar array with the charging environment of GEO. We then present the results of the laboratory tests. Finally, we conclude with suggestions of future work.

Experiment

Vacuum Chamber and Electron Beam

Figure 2 shows the diagram of the experimental setup. The length and diameter of the stainless-steel vacuum chamber are 1.2 and 1 m, respectively. The subchamber of 0.4-m length and diameter is connected to the main chamber through a gate valve. To simulate the operational temperature of 40°C at GEO, we use infrared lamps inside the chamber. The solar array test coupon is placed inside the chamber so that its face is parallel to the chamber axis. The provision is made to connect the different strings of the array to the flange of the chamber, through which all of the electrical connections to

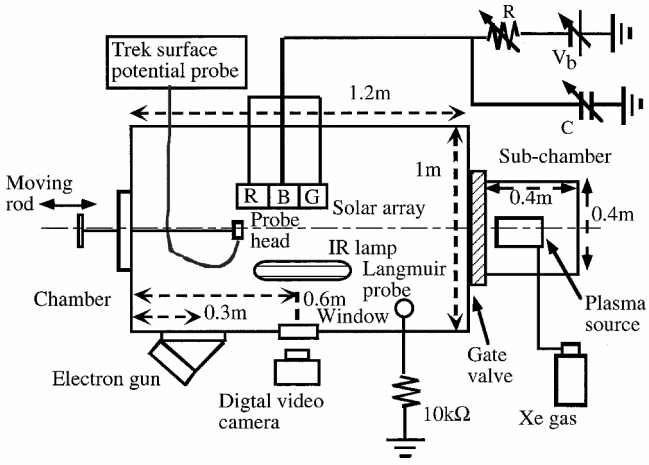

Fig. 2 Schematic of experimental setup.

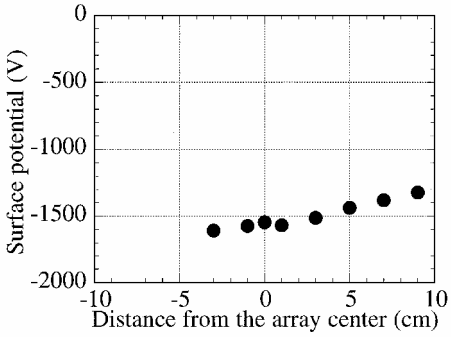

Fig. 3 Distribution of potential on the solar array surface.

the array are made. The thermocouple is attached at the backside of the array to monitor the temperature of the array, and it is also connected to the flange. The background neutral density during the experiment is between 4.0×10^{16} and 1.4×10^{17} m^{-3}. In other words, the background pressure is between 1.2×10^{-6} and 4.3×10^{-6} torr. The neutral density is higher than the values expected for typical on-orbit (GEO) conditions, At the extremely worst condition, however, the neutral density near the ETS-VIII array increases to on the order of magnitude of 10^{18} m^{-3}, when the solar array is downstream of the 22-N thruster for east–west control at an angle of 45 deg.

Electron beam irradiation on the solar array surface to study the charging phenomenon is a well-known technique to simulate GEO conditions in ground-based experiments, for example, Refs. 11–13. The electron gun, which is capable of producing electron beam of energy up to 30 kV, is fixed at the vacuum chamber. The electron beam has a half-width of approximately 5 cm at the array position. At an energy of 2.5 kV, the beam current density is in the range of 30 $\mu A/m^2$ and is about 3 mA/m^2 at 15 kV at the array potion.

The potential at the surface of the array is measured using a noncontacting surface potential probe. The probe is capable of measuring the potential in the range of ±20 kV. To measure the accurate value of the surface potential of the coverglass, the gap between the solar array surface and the surface potential probe surface is fixed at 5 mm. Every time before starting the experiments, we align the distance between the array and the surface potential probe surface using an He–Ne laser beam. In Fig. 3, we show an example of potential distribution along the solar array surface, when the beam energy is 2.5 kV and the sample is biased to −2.0 kV. The potential probe was scanned along string B. Typical errors associated with the surface potential measurement are less than 30 V. This measurement was made when arcing occurrence was relatively quiet. It is seen that the surface is uniformly charged within ±100 V over the distance of 15 cm. The output of the surface potential probe is connected to the chart recorder to record the time dependency of surface potential of the coverglass on the chart paper. We place an aluminum langmuir probe of 3-cm diam inside the chamber to measure the scale of discharge current by measuring the voltage across the 10-kΩ resistor using a passive probe (10:1). Once an arc occurs at the array, the

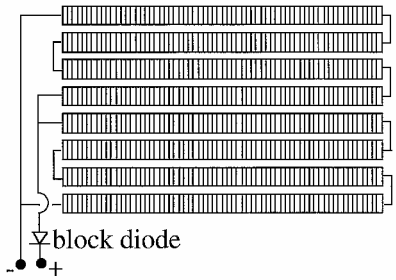

Fig. 4 Layout of ETS-VIII solar array strings.

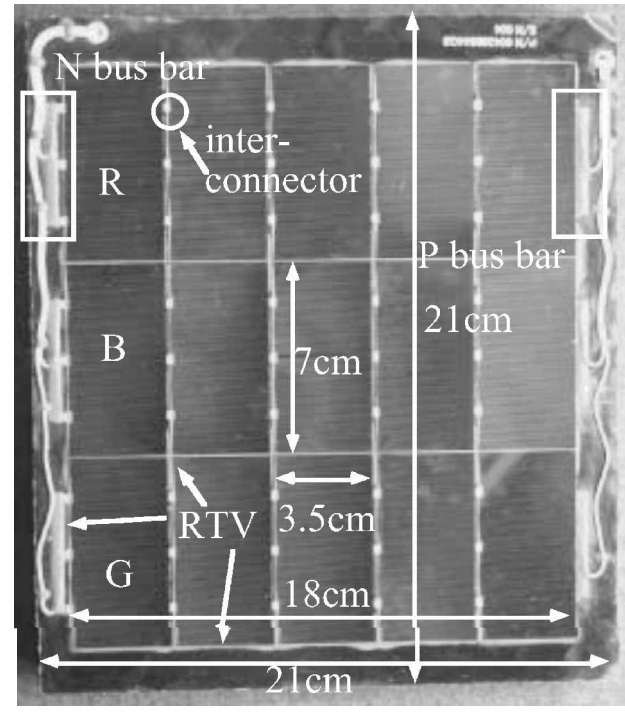

Fig. 5 Photograph of solar array coupon used in experiment.

electrons are ejected and collected by the langmuir probe. Arc positions on the solar arrays are identified using the images taken by a digital video camera.

Solar Array Coupon

The ETS-VIII has 88 strings (two wings), each with 262 Si integrated bypass function solar cells. Each string produces the output voltage of 110 V and is placed as 4 rows of 66 cells. Two parallel strings are connected in the harness with a block diode at the positive end in the power control unit. The gaps between adjacent cells are potted with nonconductive room temperature vulcanization (RTV) silicon adhesive. Each string will produce approximately 1.32-A current in the predicted maximum conditions such as noon, beginning of life, and others. The ETS-VIII array layout has adjacent cells with 55-V maximum potential difference with the maximum current capability of 2.64 A. The layout of two array strings is shown in Fig. 4. The cover glass will be made of blue red reflection (BRR)/s-0213 with the thickness of 100 μm, and the coating of oxidized zirconium (ZrO_2). The capacitance value of the coverglass and the adhesive of one string (262 cells) of the solar array is 180 nF. ETS-VIII consists of two wings of solar arrays. Each wing has 44 array strings and 8-μF coverglass capacitance.

A photograph of the solar array coupon used for the present study is shown in Fig. 5. The test coupons have been made using the same procedure as the flight product. We have made 11 such test coupons. Five coupons represent pre-1997 design, where no RTV grouting between strings was made. Six coupons represent after-1997 design, where RTV grouting was made. In the present paper, we report the tests only on the coupons with RTV grouting. In another test in plasma environment,[14] the coupons without RTV grouting have been also used.

Table 1 Experimental parameters

Case no	Purpose	Beam energy, kV	Array bias, kV	External capacitance, nF	Neutral density, 10^{17} m^{-3}
1	Inverted potential gradient	15	NA	NA	1.1
2	Arc inception threshold	2.5–4.5	−2−−3	1	0.54
3	Arc current	3–5	−0.95	20	0.99
4	Interstring sustained arc	2.4–3.5	−1.4	180–1800	0.87–1.4
5	String–substrate sustained arc	4–5	−3	200	1.1

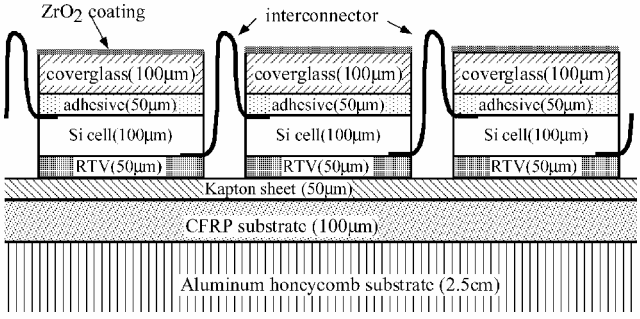

Fig. 6 Cross-sectional view of the array used in the experiments and thickness of each component.

The solar array coupon contains three strings, and we call the strings R, B and G, respectively. Each string consisted of five Si cells (3.5 × 7 cm each) of thickness of 100 μm. The cells are mounted on the Kapton substrate of thickness of 50 μm having the capacitance of 60 pF per cell. The Kapton film is mounted on a carbon fiber-reinforced plastic (CFRP) face sheet substrate (0.1 mm thick) on the top of aluminum honeycomb plate (2.5 cm thick).

The solar array string terminals are connected to the cables through the bus bars, which are coated with RTV. The cable of each string is shortened and connected to the high-voltage feed through at the chamber wall. Figure 6 shows a schematic of the cross-sectional view of an array string. The thickness of the each component is also given in Fig. 6.

No special treatment on the array surface is done after the array coupons have been shipped from the factory to the laboratory. Each time an array coupon is exposed to atmosphere, the coupon is baked at a constant temperature of $70 \pm 1^{\circ}$C at least for 2 h in vacuum ($<10^{-4}$ torr). Then, to remove the residual charge on the array surface, Xe plasma of density $\sim 10^{11}$ m^{-3} made by the plasma source placed at the subchamber is introduced into the main chamber. The insulator surface potential quickly reaches near zero potential $< \pm 30$ V within 10 s. The array temperature during the experiment is kept at $40 \pm 1^{\circ}$C.

Experimental Setup

In Table 1, we list the parameters and setting of each case of the experiment. In Fig. 7, we show the diagram of experimental circuit used for each case. The purpose of the first case is to verify the concept of the inverted potential gradient on the solar array, where the entire array coupon is floating from the chamber ground. We connect strings R, B, and G of the array and the substrate to the same potential ϕ_{ic}, as shown in Fig. 7a. We measure the structure potential ϕ_{ic} and the potential at the surface of the coverglass, ϕ_{cg}. In this case, the structure potential is the same as that of potential of the interconnector. In real spacecraft, the exposed conducting surface that is usually connected to the satellite body has a large area comparable or larger than the total area of the solar array coverglass. The exposed conducting surface consists not only of exposed interconnectors but also of much larger radiator, thermal blanket, or antenna. To give a large collection area to the interconnector and the structure, we attach a copper plate of 23.6-cm length and 6 cm-width to the side of the solar array, so that it makes contact with the substrate of the array.

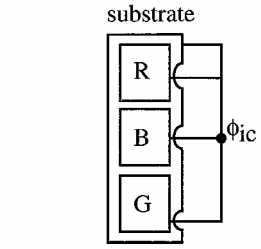

a) Case 1

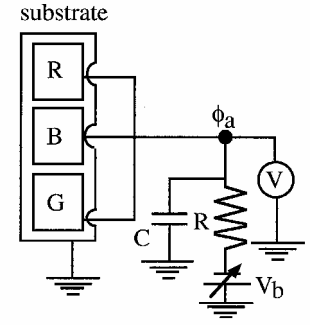

b) Case 2: $R = 10$ MΩ, $V_b = -2 \sim -3$ kV, and $C = 1$ nF

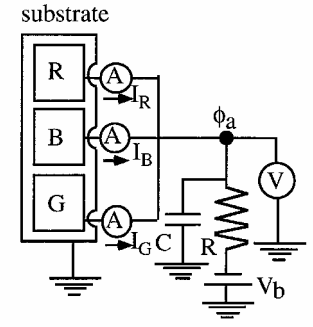

c) Case 3: $R = 100$ kΩ, $V_b = -950$ V, and $C = 20$ nF

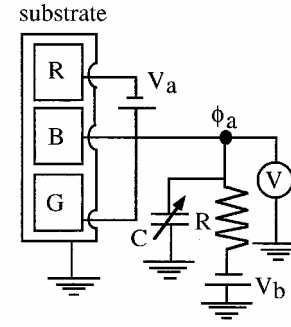

d) Case 4: $R = 10$ MΩ, $V_b = -1.4$ kV, and $V_a = 55$ V

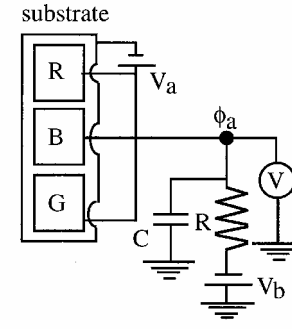

e) Case 5: $R = 10$ MΩ, $V_b = -3$ kV, $V_a = 110$ V, and $C = 200$ nF

Fig. 7 Circuit setup for each case listed in Table 1.

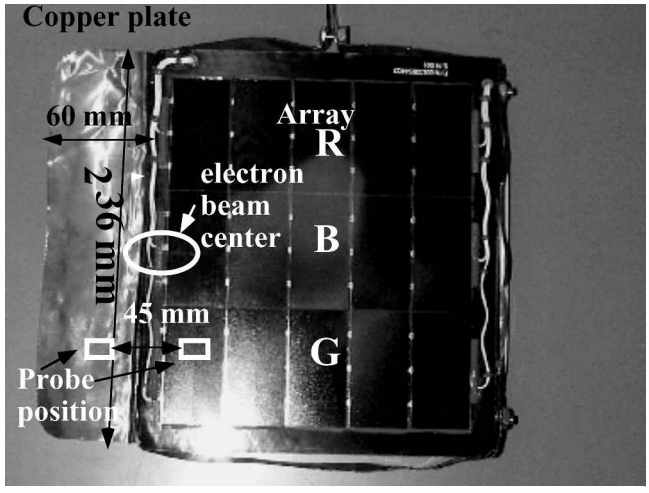

Fig. 8 Photograph of solar array attached with copper plate to increase conductive area simulating spacecraft body for case 1 experiment.

A photograph of the solar array with the copper plate is shown in Fig. 8. The copper plate and the substrate are floating from the chamber ground. The center of electron beam (15 kV) and the position of surface potential probe are also shown in Fig. 8. The structure potential ϕ_{ic} and the surface potential of the coverglass, ϕ_{cg}, are measured by the surface potential probe at the copper plate and the array surface, respectively. We irradiated the array coupon using an electron beam, so that the beam spot falls on both the copper plate and the array surface as also shown in Fig. 8. The surface potential probe is placed at one particular place in front of the copper plate, that is, 4 cm from the edge of the copper plate, to measure the potential of the body surface. The surface potential of the coverglass is measured by placing the surface potential probe in front of string G at 2.5 cm from the edge of the string. The output of the surface potential probe is connected to the chart recorder to record the time-varying potential of the structure and the coverglass. Throughout the experiment case 1, the surface probe is always operating, even before the electron beam is turned on and while the beam is running.

The threshold potential difference for arc initiation between the coverglass and the interconnector is measured in case 2. The circuit setup is shown in Fig. 7b. We place the surface potential probe at the center of string R of the array. We bias the solar array to a high negative potential from -2 to -3 kV using a high-voltage power supply, connected through a 10-MΩ resistor. We use 1 nF as the external circuit because the voltage limit of this capacitor is very high (up to 50 kV), for the same reason we use 10-MΩ resistor. To identify the arc position, the video images of array surface is recorded by a digital video camera. The array potential ϕ_a is measured using a high-voltage (HV) probe. The HV probe and output of the surface potential probe are connected to a four-channel oscilloscope (100 MHz) that is triggered by the rise of the HV signal. During the measurement, the surface potential probe is mostly fixed over a coverglass at the center of the array coupon. The probe might block some fraction (approximately 10%) of the electron beam coming to the surface. Because the beam hits the surface obliquely, however, the beam should be able to charge the coverglass surface. We have scanned the array surface moving the probe and confirmed that the array surface has been uniformly charged as shown in Fig. 3.

The circuit setup for the arc inception phenomenon (case 3) is shown in Fig. 7c. We bias the solar array sample at a negative bias voltage of -950 V using a power supply connected to the array through 100-kΩ resistor. We measure the currents to strings R, B, and G, I_R, I_B, and I_G, of the array using current probes. The array potential ϕ_a is monitored using the HV probe. The current probes and the HV probe are connected to the oscilloscope that is triggered by the rise of HV probe signal. We use an external capacitance of 20 nF to give enough energy to each arc so that its optical signature can be recorded by the video camera to identify the position of each arc.

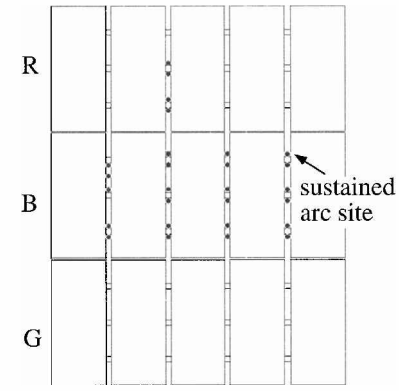

Fig. 9 Interconnectors and •, positions of damage made on array coupon.

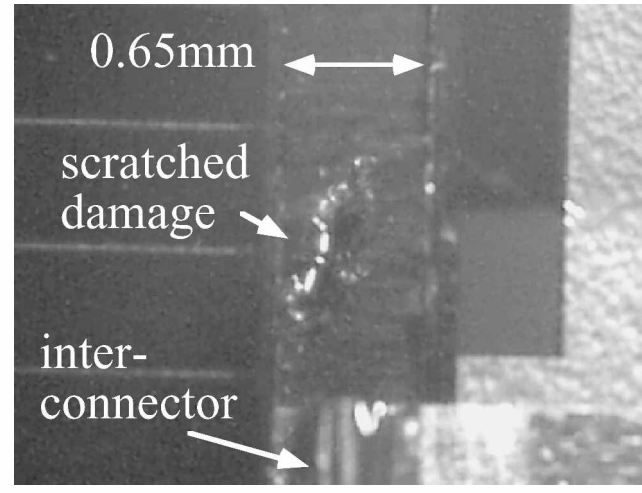

Fig. 10 Magnification of sustained arc site before the experiment; position on array coupon shown in Fig. 9.

The circuit setup for the test of the interstring sustained arc phenomenon (case 4) is shown in Fig. 7d. To simulate the potential difference between the adjacent strings, we apply the potential difference V_a of 55 V between the strings R and B using a floating power supply at the external circuit. The maximum current I_{max} to flow is limited to 2.64 A. The power supply works as a constant voltage supply. However, at the time of a short circuit such as the sustained arc, it works as a constant current supply with the maximum current limited to a preset value, 2.64 A for the present case. We bias the solar array strings at -1.4 kV, V_b, using an HV power supply. The bias voltage of -1.4 kV is chosen because the voltage limit of each capacitance is 1.6 kV.

We insert an additional capacitance in the external circuit to simulate the capacitance value of several strings of the array, where the energy release of each arc is as high as 1.8 J. The array potential ϕ_a is measured using an HV probe. We measure the scale of each arc via the signal received by the langmuir probe and the video image. The HV probe and the passive probe connected to the langmuir probe are connected to the oscilloscope, which is triggered by the rise of the HV probe signal.

In case 5, we study the string–substrate sustained arc formation through the damaged Kapton insulator. We test two coupons. One coupon has no obvious physical damage on the Kapton sheet. The other has the damage on the Kapton substrate near the interconnectors of strings B and R. The damage is made by scratching the Kapton surface four or five times with a penknife. The points of damage on the Kapton are shown in Fig. 9 and a magnified photograph is shown in Fig. 10. The experimental circuit for the measurement is shown in Fig. 7e. ETS-VIII array has an output voltage of 110 V. The interconnector at the positive end of the array has a positive potential of 110 V with respect to the substrate, whose potential is equal to the satellite body potential. To simulate the potential difference

between the substrate and the positive end of the solar array string, we apply the potential difference V_a of 110 V between the substrate and the three strings using the floating power supply at the external circuit. The maximum current I_{max} to flow is limited to 2.64 A. We bias the solar array strings to −3 kV, V_b using the HV power supply. Bias voltage of −3 kV has been selected to give enough energy to each arc. Because the voltage limit of the capacitor was −1.6 kV, we used two pairs of 200-nF capacitance connected in series, and one pair contains two capacitors connected in parallel.

Results and Discussion

Inverted Potential Gradient

Figure 11 shows the chart recorder drawing of the potential measured using the surface potential probe at the coverglass surface and the copper plate at the beam energy of 15 kV at the neutral density of 1.1×10^{17} m^{-3}. Before the emission of the electron beam, the potential at the surface of the copper plate was nearly 0 V. Once we switched on the electron beam and the beam was emitted on both the body and the coverglass, the potential of the body dropped suddenly to about −9.0 kV within a second. This potential further decreased gradually to −9.6 kV within 10 s after the beam was on, and the potential remained almost the same up to 20 s. In this short time, there were many trigger arcs on the array surface. The trigger arcs appear as downward spikes in Fig. 11. When we moved the surface potential probe in front of the coverglass of string G of the array, the potential increased from −9.6 to −8.6 kV. Therefore, the coverglass potential was less negative than the interconnectorby about 1 kV. This result is the first experimental verification made in a simulated GEO environment that the inverted potential gradient condition really occurs if certain conditions are met.

Trigger Arc Inception

Producing the inverted potential gradient only by the electron beam requires the array circuit to be floating, which makes the measurement difficult and dangerous. Therefore, for the rest of the paper we produce the inverted potential gradient by biasing the solar array circuit at a highly negative potential using an HV power supply at the external circuit and irradiating the electron beam on the coverglass surface so that it will emit secondary electrons and be less negatively charged than the interconnector.

In Table 2 we list the differential voltages between the coverglass and interconnector when arcs occurred under various conditions. Arcs were observed at the edge of solar cell, mostly interconnectors, and their position were identified by the video images. Although arcs occurred on any edge of solar cell, in Table 2 we list only the cases where the arc position was within 8 cm from the surface potential probe, considering the small nonuniformity of the potential distribution over the array surface. Arcs occurred when the differential voltage between the coverglass and interconnector reached approximately 400 V. In Fig. 12, we show the transient of surface potential probe signal and the array potential. For this example, the arc occurred 8 cm away from the surface potential probe. It is clear that, before the arc, there is potential difference of 380 V and that the difference quickly decreases within 10 μs after arc onset. The

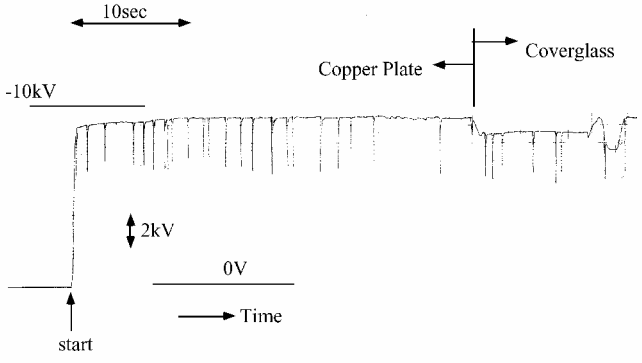

Fig. 11 Chart recorder of surface potential of the array and copper plate measured using surface potential probe in case 1; electron beam energy is 15 kV.

Table 2 List of differential voltages at the arc inception

Beam energy, kV	Array potential ϕ_a, kV	Coverglass potential ϕ_{cg}, V	Differential voltage $\Delta V = \phi_{cg} - \phi_a$, V	Distance from the surface potential probe, cm
2.5	−2	−1649	351	6.5
2.5	−2	−1639	361	7.0
2.5	−2	−1616	384	8.0
3.5	−2.5	−1235	1265	6.0
3.5	−2.5	−1730	770	7.0
2.5	−3	−660	2340	3.5
2.5	−3	−1000	2000	7.0
4.5	−3	−742	2258	7.0

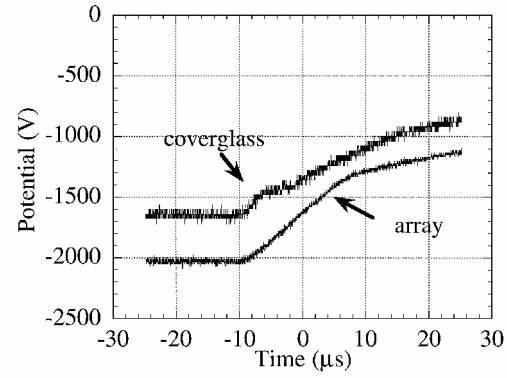

Fig. 12 Example of waveforms of coverglass surface potential and array potential at arc inception measured in the case 2 experiment.

NASCAP simulation[9] predicted 2.9 kV during eclipse and 1.2 kV during local morning as the maximum differential voltage under the worst substorm condition. The simulation, however, did not take into account the trigger arc that could nullify the potential difference. When the large area of the real solar array, approximately 60 m^2, compared to the test coupon, 0.037 m^2 is considered, it is possible that a trigger arc occurs at some point on the array before the potential difference builds up to such a large value, larger than 1 kV.

Figure 13 shows the typical waveforms measured in the oscilloscope. In this case, the arc occurred at B string. Once an arc occurs, the array potential increases due to the voltage drop across the 100-kΩ resistance as shown in Fig. 13d. At the string where the arc occurs, a positive current flows from the string toward the ground, which is called discharge current I_B, the waveform of which is shown in Fig. 13a. At the same time, negative currents I_R and I_G are flowing from strings R and G of the array, which are called as neutralization currents, and those are shown in Figs. 13b and 13c.

Note from Fig. 13 that, once the arc occurs at string B of the array, the coverglasses of strings R and G are supplying energy to the arc point. There is a current path between the arc point on string B and the coverglasses on strings R and G through the arc plasma and the external circuit. It is essentially RC discharge, where R is the resistance of arc plasma and C is the capacitance of the coverglass. The charges stored in the coverglass before the arc is released and supplied as a discharge current. The total charge flown in the arc at string B shown in Fig. 13 is about 1.0×10^{-6} C. For an arc at string B, the capacitance of the coverglass of the strings R and G are supplying the energy. If both strings R and G are fully charged, they can provide 6.5×10^{-6} C.

The coupling between the arc point and the coverglass capacitance was previously observed in LEO plasma environment,[15–17] where the plasma and neutral densities were of the order of magnitude of 10^{11} and 10^{19} m^{-3}, respectively. The current flow shown in Fig. 13 indicates that, even at low neutral density of 9.9×10^{16} m^{-3} and in the absence of ambient plasma environment, the coupling between the arc site and the nearby coverglass occurs and that the coverglass supplies its energy to the arc. The electrical conductivity of the ambient plasma is much lower than LEO environment for the present case. Once an arc occurs, the arc plasma provides the necessary conductivity. Therefore, once an arc occurs due to the inverted

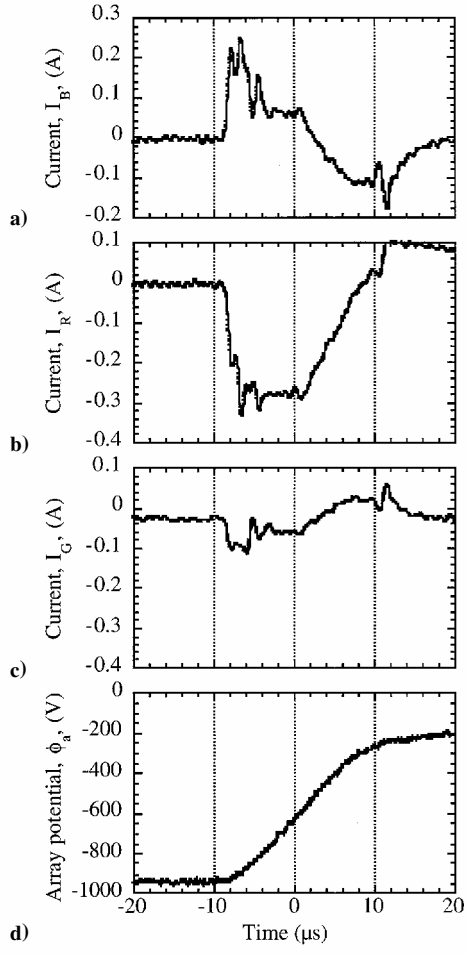

Fig. 13 Measurement at arc inception in case 3 experiment example of typical waveforms: a) discharge current, b) string R neutralization current, c) string G neutralization current, and d) array potential.

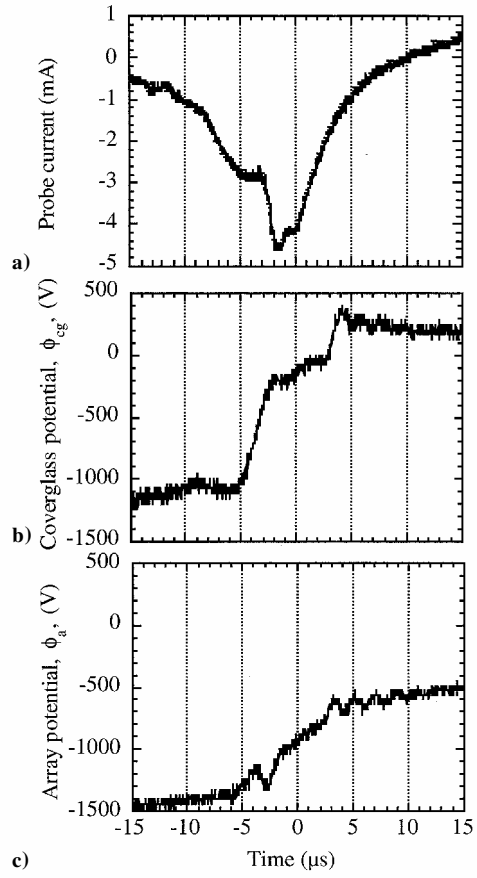

Fig. 14 Arc inception measured in case 4 experiment example of waveforms of a) current to the lagmuir probe, b) coverglass surface potential, and c) array potential.

potential gradient, the growth mechanism of the arc plasma is the same as in LEO environment, although its extent might be different. A similar phenomenon has been also observed recently in Ref. 13 in a simulated GEO environment.

Interstring Sustained Arc

A pulse of the arc discussed in the preceding section may trigger the sustained arc between the solar cells at a large potential difference. As noted earlier, the arc plasma first grows by receiving the energy stored on the coverglass as electrostatic energy. For a given set of the potential difference and the distance between two strings, whether a trigger arc plasma makes the transition to the sustained arc probably depends on the initial conductivity when it bridges the two strings. That conductivity is determined by the energy, which the arc plasma receives from the coverglass capacitance. Before we carry out the test on the sustained arc, how many coverglasses contribute to the growth of arc must be known to define adequate experimental conditions. In a laboratory experiment, the coverglass capacitance is usually simulated by inserting capacitance into the external circuit because the size of a vacuum chamber limits the number of solar cells placed inside the vacuum. The amount of capacitance, however, is still a topic of ongoing controversy, mostly because no one has yet demonstrated experimentally how many coverglasses are involved in one trigger arc in a GEO environment. In a LEO environment, an experiment by Cho et al.[17] has shown that one trigger arc influences the coverglass within a 4-m distance. However, in a GEO environment, where the ambient plasma conductivity is many orders of magnitude smaller than a LEO environment, the number derived in Ref. 17 only serves as a reference regarding the upper bound on the capacitance value.

In the present study, we have chosen to increase the external capacitance from 180 to 1800 nF step-by-step until we see the sustained arc. The value of 180 nF has been chosen because one string of the ETS-VIII solar array has a capacitance of 180 nF. We biased the array to -1.4 kV. Then the capacitance of 1800 nF can provide an arc energy of 1.8 J. From the result of the case 2 experiment, a trigger arc can occur when the differential voltage of 400 V is built up between the coverglass and the cell. ETS-VIII has two wings of solar array with a capacitance of 8 μF per wing. If the two full wings supplies energy to the arc at the differential potential ΔV of 400 V between the body and the coverglass, the energy release is about 1.3 J. Therefore, if we do not see the sustained arc up to 1800 nF, we can conclude that the sustained arc will not occur even at worst case in orbit.

Figure 14 shows the typical waveforms measured in the case 4 experiment at the external capacitance of 360 nF at the neutral density of 1.1×10^{17} m^{-3}. In Fig. 14, the beam energy is 3.2 kV. The probe current measured as the voltage across the 10-kΩ resistor is shown in Fig. 14a. Once an arc occurs at the array surface, electrons are ejected and are collected by the probe, showing the negative signal. Surface potential of the coverglass ϕ_{cg} measured using the surface potential probe over the second cell from the right of string B is shown in Fig. 14b. The bias potential ϕ_a is shown in Fig. 14c. The probe signal and the video images are used to infer the scale of each arc. The langmuir probe output indicates that a significant number of electrons is ejected. The probe is located approximately 40 cm from the array surface. When it is assumed that electrons are ejected semispherically from the arc point, the cross-sectional area of the 3-cm-diam probe occupies only 0.07% of the semisphere of radius 40 cm.

Figure 15 shows the probe negative peak signal measured by the langmuir probe during the arc on the solar array surface at various values of the external capacitance. Each point is an average of at least 4 measurements and a maximum of 11 measurements. Error bars indicate the standard deviation. The probe negative peak signal is seen to increase with the increase in the capacitance, indicating that the scale of the arc is increasing with the increase in the additional

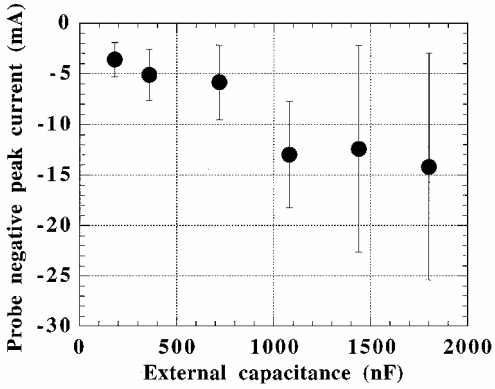

Fig. 15 Dependence of the probe signal peak I_p on external capacitance.

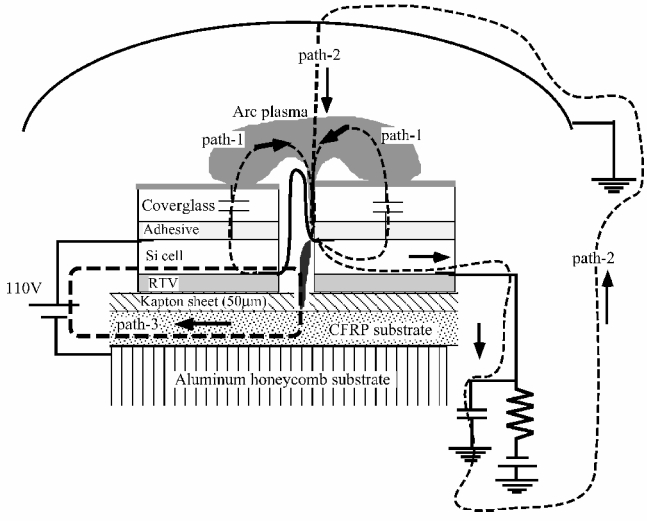

Fig. 16 Model of formation mechanism of string–substrate sustained arc between interconnector and substrate through damage in Kapton.

capacitance, which supplies the energy to the arc. The brightness also increases as the external capacitance increases. Note that, at higher capacitance values, for example, at 1800 nF, and at the bias voltage of −1.4 kV, the maximum probe current is 0.025 A, which corresponds to approximately 36 A of the arc current.

We observed 42 trigger arcs during the experiment of about 4 h. Among those, 13 arcs were with 1440-nF capacitance and 4 arcs were with 1800-nF capacitance. Even with the energy exceeding 1.3 J, we did not observe sustained arc. The test coupon had RTV silicon grouting between strings. Probably the grouting worked by making the distance between the trigger arc spot and the nearest exposed conductor of a different string longer than the necessary distance. The minimum distance between the exposed conductor of two different strings is 2 cm for the present case. In conclusion, the solar array design tested in the present experiment can prevent the interstring sustained arc when it is operated at the maximum interstring potential difference of 55 V and the current capability of 2.64 A.

String–Substrate Sustained Arc

A model for the string–substrate sustained arc formation between an interconnector and the substrate is shown in Fig. 16. The potential difference between the interconnector of the most positive end and the CFRP substrate is 110 V with current capability of 2.64 A. Because of the development of an inverted potential gradient on the array, an arc occurs at the interconnector. Once a trigger arc occurs, it receives its energy from the nearby coverglass, whose current path is denoted as path 1 in Fig. 16. The arc current also flows through the capacitance connected in the external circuit to the chamber wall and closes the current path. This path is path 2. Dense plasma is created at the arc site and is in contact with the CFRP substrate through the

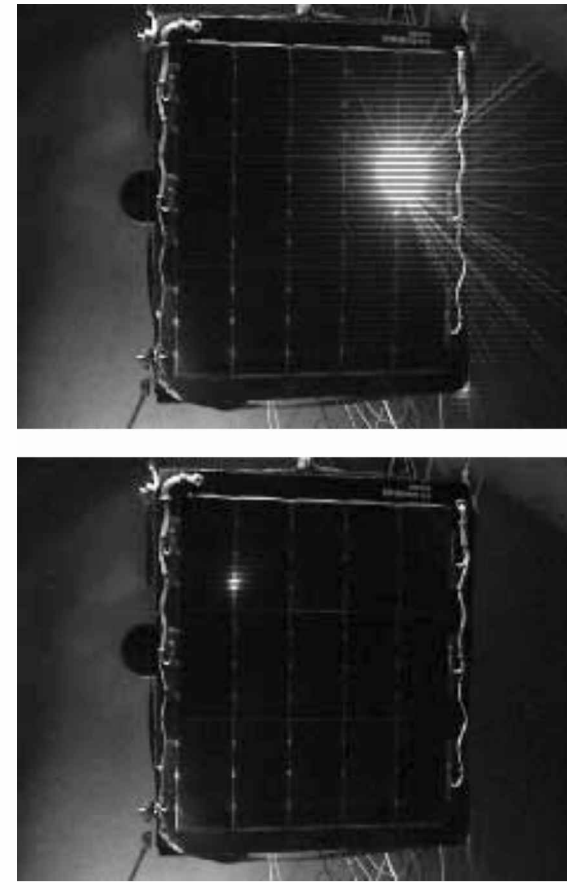

Fig. 17 Video images of a) arc occurring at an interconnector with damage nearby and b) an interconnector without damage.

defect in the Kapton insulator on which the cells are mounted. Then the current path will be formed between the interconnector and the CFRP substrate. The arc is sustained by the power supply and leads to the destruction of the array circuit. This current path is shown as path 3.

The test on the string–substrate arc was carried out by biasing the array coupon at −3 kV instead of −1.4 kV because we wanted to increase the arc rate by increasing the beam current that increased with the beam energy. At the same time, the external capacitance was lowered to 200 nF so that the energy stored in the system capacitance stays at 0.9 J, corresponding to the energy of one wing of solar array. We increased the beam energy to 4–5 kV, and the bias voltage had to be changed to produce the inverted potential gradient due to the secondary electron emission from the coverglass. During the experiment, the beam energy was tuned so that arcs occurred more often.

Before we carried out the test with the array coupon shown in Fig. 9, the test was done with only two cracks on the Kapton sheet. We observed total 43 trigger arcs with −3-kV bias, but there was no sustained arc. Then we increased the number of cracks to 27, as shown in Fig. 9, and carried out the second test. There were total 54 arcs during 100 min of the second test. Figure 17 shows video images of a trigger arc occurring at an interconnector with a crack nearby (Fig. 17a) and a trigger arc at an interconnector without a crack (Fig. 17b). Some of the trigger arcs occurred at the interconnectors without a crack nearby. When the trigger arc occurred at such a place, the intensity of the flash associated with the arc was always much lower than that associated with the arc that occurred at the interconnectors with crack nearby. This result suggests that an arc near the crack actually short circuited the string and the substrate for a short period of time and extracted the energy from the external power supply but failed to maintain itself.

The sustained arc between string B and the substrate finally occurred as the 54th arc. The power supply between the string and substrate acted as a constant voltage (110 V) source before the

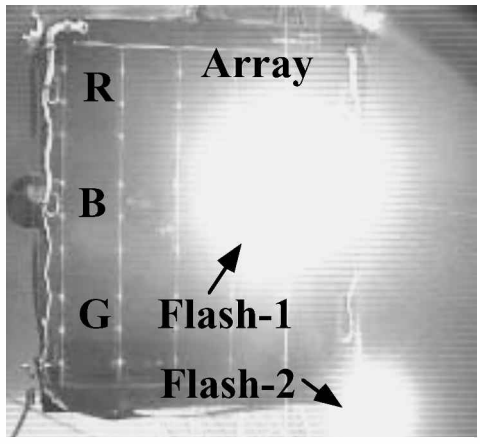

Fig. 18 Video image of string–substrate sustained arc (flash 1) observed in case 5 experiment.

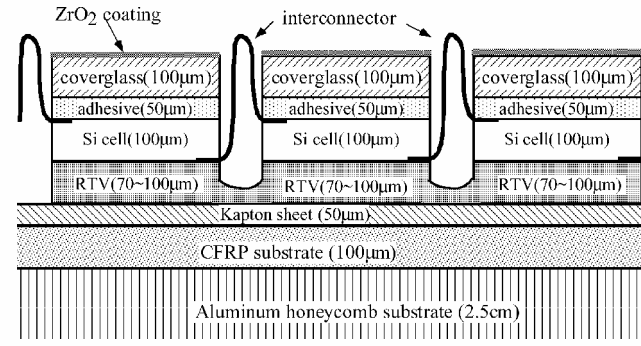

Fig. 19 Cross-sectional view of the modified array and thickness of each component.

sustained arc. Once the sustained arc occurred, its voltage collapsed and it became a constant current source of 2.64 A. The arc was not steady though. It repeated on and off during 19 s with an approximately 1-s interval until the floating power supply was switched off. The reason why the arc was unsteady is probably because the current of 2.64 A was not sufficient to maintain the steady dc arc current. The sustained arc is shown in Fig. 18. The sustained arc was formed between the string B and the CFRP substrate through the crack intentionally made on Kapton film. The electron beam energy was 4.1 kV, and the bias voltage was -3 kV at the neutral density of 1.1×10^{17} m^{-3}. From Fig. 18, it is seen that a sustained arc occurred between the interconnector and the CFRP substrate (flash 1) and an arc also occurred between the CFRP substrate and the chamber wall (flash 2).

Among the 54 arcs observed in the second test of case 5, flash 2 at the edge of the substrate was always accompanied when bright flash such as that in Fig. 17a occurred at the interconnector with a nearby crack. Flash 2, however, never occurred alone nor accompanied smaller flashes as in Fig. 17b. Inspection of the site of flash 2 after the experiment revealed that flash 2 was due to arcs at the edge of the Kapton sheet and the substrate. Because the substrate also had a negative potential of -3 kV, once dense plasma was generated due to the arc near the Kapton damage and released to the chamber, the array was surrounded by the relatively dense plasma. Then, if the substrate voltage recovered to the order of magnitude of -100 V, an arc could occur at the edge of the Kapton sheet like an arc in LEO plasma environment. Therefore, flash 2 is the result of an arc at the array interconnector, not the cause of it.

Observation by an optical microscope of the the sustained arc site after the experiment has revealed that the arc has damaged the interconnector, solar cell material, and the Kapton film on the CFRP substrate. The interconnector had two legs to connect the adjacent cells, but one leg has been completely blown off. The cells and the coverglass near the arc site have been melted. The array open-circuit voltage after the experiment has decreased to 2.6 V from the 3.1 V that was measured before the experiment. The difference corresponds to the output voltage of one cell, which means that the damaged cell has short circuited within the cell. The resistance between the damaged string and the substrate is only 2 kΩ. This resistance cannot sustain even 10 V. When it is considered that the string–substrate sustained arc is likely to occur near the positive end of array string where a voltage of 100 V is applied between the string and substrate, the damaged string cannot provide its power once the sustained arc occurs in orbit.

Without damage made before the experiment, the string–substrate arc will not occur under the worst condition for ETS-VIII. As suspected in Ref. 8, it had been originally thought that repeated trigger arcs might lead to the damage on the Kapton sheet near the interconnector. We analyzed the test coupon used in the case 4 experiment, where many arcs occurred with a large amount of energy $\sim$1 J. Although significant darkening of the Kapton sheet near arc spots was observed, an electron microscope picture of 600× resolution revealed no damage on the Kapton surface. Also, the inspection by an infrared microscope (BIO-RAD F45RD-UMA30A) showed no change in the molecular structure of the Kapton sheet.

To confirm that the string–substrate sustained arc does not occur with healthy Kapton sheet, we tested a coupon with no obvious physical damage on the Kapton sheet. Before the test, all of the area around the cells was inspected by a 60× microscope, and no defect on the Kapton sheet was found. We irradiated an electron beam on the test coupon for 10 h with the circuit setup of Fig. 7e. Although we observed 194 trigger arcs, the string–substrate sustained arc did not occur.

The fact that string–substrate arc occurred only when Kapton was already damaged suggests that if care is taken not to damage the Kapton sheet on the ground, we can reduce the risk of string–substrate sustained arc significantly. The cause of damage in orbit is probably only the impact by debris or micrometeoroids. The hypervelocity impact probability for a GEO satellite is very difficult to calculate because reliable data for the population of meteoroids and debris, especially of small sizes less than a centimeter is necessary. See Ref. 18, where the impact probability due to annual meteor showers (debris not included) was calculated.

Proposal of Modified Design

It is most likely that the damage to the Kapton sheet occurs when attached cells are removed for repair or exchange. Therefore, the damage can be detected by thorough inspection near the repaired or exchanged cells. As one additional mitigation against the possible damage to the Kapton sheet, we propose a design shown in Fig. 19. The array design that we have used in the present study for the tests has a RTV layer of thickness of 50 μm between the cell and the Kapton substrate and no RTV below the interconnector (Fig. 6). In the modified design, the Kapton layer under the interconnectors is also coated by RTV, which leaks out from the bottom of the cell. To leak RTV, its thickness has been increased to 100 μm at maximum. Increasing the thickness of RTV from 50 to 100 μm gives the additional mass of approximately 40 kg. In addition, extensive coating by RTV around the bus bars is carried out to suppress the trigger arcs. The coating around bus bars is much easier compared to the coating of interconnector, because the requirement for the stress relief against the thermal cycle at a bus bar is not as severe as that at an interconnector.

Conclusions

Laboratory tests on 110-V solar arrays to be used onboard ETS-VIII have been carried out in a simulated GEO environment. We have focused our tests on the inverted potential gradient concept, that is, the potential of the coverglass of the array less negative than the conductive body. We have tested solar array coupons with RTV grouting between the strings and the bus bars coated with RTV. We have verified the inverted potential gradient by irradiating the solar array coupon via an electron beam, where the array is completely floating from the chamber ground. The maximum potential difference of approximately 1 kV has been observed between the coverglass and the cell, and we have observed many arcs at this potential difference.

We have carried out the experiment by creating the inverted potential gradient on the solar array by biasing the array to a highly negative potential (of the order of magnitude of 1 kV) with an HV power supply and by making the potential of the cover glass less negative than that of the cell. An arc has occurred on the solar array once the potential difference of about 400 V has built up between the coverglass and the conductor. Measurement of the arc current has revealed that the arc inception in the inverted potential gradient is similar to arc inception in a LEO environment, where the arc plasma grows by extracting the charge stored on the nearby coverglass surface.

We have tested whether a sustained arc occurs between adjacent cells of the solar array with a potential difference of 55 V and a current capability of 2.64 A. The arc plasma has been given energy as high as 1.8 J, but it has never become a sustained arc between the strings.

A different type of sustained arc phenomenon has been observed between the interconnector and the CFRP substrate through the intentionally damaged Kapton insulator with the potential difference of 110 V and the current capability of 2.64 A. This sustained arc has short circuited, between the interconnector of the positive end of the array and the CFRP substrate and led to the destruction of the solar array circuit. We have proposed an array design to mitagate against the damage to the Kapton insulator, where RTV is leaked out from the bottom of cell to cover the Kapton sheet near the interconnector. To implement the mitigation plan, the thickness of RTV grouting between the cell and the Kapton sheet has been increased from 50 to 70–100 μm.

During the present study, many problems surfaced regarding studying arcing in a GEO environment. The adequate value of the external capacitance simulating the coverglass giving the energy to the arc plasma must be determined. For that purpose, the growth process of the arc plasma in a GEO environment should be studied in future. The concept of the inverted potential gradient has been verified in the present laboratory experiment. To verify the inverted potential gradient in the orbital environment, it has been decided to mount a potential monitor (POM) on ETS-VIII. The POM will carry three typical coverglass materials as charging samples, BRR/s-0213, CMX-BRR, and CMG-AR, and measure the differential voltage between the insulator surface potential and the satellite ground. Analysis of the flight data correlating with the ambient GEO plasma environment will provide the data helpful to design future satellites.

Acknowledgments

The authors thank the members of Toshiba Corp., Japan, for the array sample fabrication and after experiment analysis. The authors acknowledge M. Hikita of Kyusha Institute of Technology, H. Kuninaka of the Institute of Space and Aeronautical Science, and H. Nishimoto of the National Space Development Agency (NASDA) for discussions and S. Kawakita of NASDA and Y. Saito of the High Energy Accelerator Research Organization for the measurement of secondary electron coefficients of the ZrO_2 coated coverglass. The authors extend their thanks to H. Fujii and N. Onodera of Mitsubishi Electric Corp. for NASCAP/GEO analysis of the Engineering Test Satellite VIII.

References

[1]Cho, M., "Arcing on High Voltage Solar Arrays in Low Earth Orbit: Theory and Computer Particle Simulation," Ph.D. Dissertation, Dept. of Aeronautics and Astronautics, Massachusetts Inst. of Technology, Cambridge, MA, Feb. 1992.

[2]Hastings, D. E., "A Review of Plasma Interactions with Spacecraft in Low Earth Orbit," *Journal of Geophsical Research*, Vol. 100, No. A8, 1992, pp. 14,457–14,483.

[3]Ferguson, D. C., Snyder, D. B., Vayner, B. V., and Galofaro, J. T., "Array Arcing in Orbit from LEO to GEO," AIAA Paper 98-1002, Jan. 1998.

[4]Hastings, D. E., and Garrett, H., *Spacecraft–Environmental Interactions*, Cambridge Univ. Press, New York, 1996, Chap. 5.

[5]Purvis, C. K., Garrett, H. B., Whittlesey, A. C., and Stevens, N. J., "Design Guidelines for Assessing and Controllling Spacecraft Charging Effects," NASA TP-2361, 1984.

[6]Katz, I., Davis, V. A., and Snyder, D. B., "Mechanism for Spacecraft Charging Initiated Destruction of Solar Arrays in GEO," AIAA Paper 98-1002, Jan. 1998.

[7]Bogus, K., Claassens, C., and Lechte, H., "Investigations and Conclusions of the ECS-Solar-Array In-Orbit Power Anomalies," *Proceedings of 18th IEEE Photovoltaic Space Conference*, IEEE Publications, Piscataway, NJ, 1985, pp. 368–375.

[8]Levy, L, Reulet, R., Sarrail, D., Siguier, J. M., and Lechte, H., "MARCES and ECS Anomalies Attempt for Insulation Defect Production in Kapton," *Proceedings of 5th European Symposium on Photovoltaic Generators in Space*, ESA, Noordwijk, The Netherlands, 1986, pp. 161–169.

[9]Fujii, H., Onodera, N., Murakami, Y., Kawakita, S., Nishimoto, H., and Takahasshi, M., "Charging Analysis of Engineering Test Satellite VIII (ETS-VIII) of Japan," *Proceedings of 7th Spacecraft Charging Technology Conference*, ESA, Noordwijk, The Netherlands, 2001, pp. 183–188.

[10]Kawakita, S., Imaizumi, M., Takahashi, M., Matsuda, S., Michizono, S., and Saito, Y., "Influence of High Energy Electrons and Protons on Secondary Electron Emission of Cover Glasses for Space Solar Cells," *Proceedings of 20th International Symposium on Discharge and Electrical Insulation in Vacuum*, Ecole d'Ingenieurs de Tours, Tours, France, 2002, pp. 84–87.

[11]Crofton, M. W., and Francis, R. W., "Electrostatic Discharge Measurements on Solar Array Coupons in a Simulated GEO Environment," Society of Automotive Engineers, 34th Intersociety Energy Conversion Engineering Conf., SAE TP 1999-01-2634, Aug. 1999.

[12]Frederickson, A. R., Benson, C. E., Cooke, E. M., "Gaseous Discharge Plasmas Produced by High-Energy Electron-Irradiated Insulators for Spacecraft," *IEEE Transactions on Plasma Science*, Vol. 28, No. 6, 2000, pp. 2037–2047.

[13]Leung, P., "Plasma Phenomena Associated with Solar Array Discharges and Their Role in Scaling Coupon Test Results to a Full Panel," AIAA Paper 2002-0628, Jan. 2002.

[14]Ramasamy, R., Cho, M., Toyoda, K., Nozaki, Y., and Takahasi, M., "Laboratory Tests on Plasma Interactions of ETS-VIII Solar Arrays," *Proceedings of 7th Spacecraft Charging Technology Conference*, ESA, Noordwijk, The Netherlands, 2001, pp. 359–364.

[15]Cho, M., Miyata, N., Hikita, M., and Sasaki, S., "Discharge over Spacecraft Insulator Surface in Low Earth Orbit Plasma Environment," *IEEE Transactions on Dielectrics and Electrical Insulation*, Vol. 6, No. 4, 1999, pp. 501–506.

[16]Cho, M., Hikita, M., Tanaka, K., and Sasaki, S., "Transient Phenomena Induced by Discharge on Solar Array in Low Earth Orbit Plasma Environment," *IEEE Transactions on Plasma Science*, Vol. 29, No. 5, 2001, pp. 789–795.

[17]Cho, M., Ramasamy, R., Hikita, M., Tanaka, K., and Sasaki, S., "Plasma Response to Arcing in Ionospheric Plasma Environment: Laboratory Experiment," *Journal of Spacecraft and Rockets*, Vol. 39, No. 3, 2002, pp. 392–399.

[18]Lai, S., Murad, E., and McNeil, W. J., "Hazards of Hypervelocity Impacts on Spacecraft," *Journal of Spacecraft and Rockets*, Vol. 39, No. 1, 2002, pp. 106–114.

D. L. Edwards
Associate Editor